Fuel 293 (2021) 120295

Contents lists available at ScienceDirect

Fuel

journal homepage: www.elsevier.com/locate/fuel

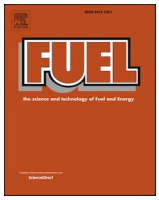

Full Length Article

Large-eddy simulation of spray assisted dual-fuel ignition under reactivity-controlled dynamic conditions

Bulut Tekgül [a,*], Heikki Kahila [b], Shervin Karimkashi [a], Ossi Kaario [a], Zeeshan Ahmad [a], Éric Lendormy [b], Jari Hyvönen [b], Ville Vuorinen [a]

[a] Department of Mechanical Engineering, Aalto University School of Engineering, Otakaari 4, 02150 Espoo, Finland
[b] Wärtsilä Finland Oy, Vaasa FI-65101, Finland

ARTICLE INFO

Keywords:
LES
Ignition
Dual-fuel
RCCI
OpenFOAM

ABSTRACT

Here, a large-eddy simulation and a finite-rate chemistry solver (see Kahila et al. Combustion and Flame, 2019) is utilized to investigate diesel spray assisted ignition of a lean methane-air mixture. A compression heating model is utilized to emulate the ambient temperature and pressure increase in a compression ignition (CI) system. The key parameter is the start of injection (SOI) relative to a virtual top dead center (TDC), where the peak adiabatic compression pressure/temperature would be achieved. Altogether, five different cases are investigated by advancing the SOI further away from the TDC with constant injection duration. The main findings of the paper are as follows: 1) Advancing the SOI advances the ignition timing of the spray with respect to the TDC from 0.91 to 7.08 CAD. However, beyond a critical point, the ignition time starts retarding towards the TDC to 4.46 CAD due to the excessively diluted diesel spray. 2) Advancing the SOI increases the contribution of leaner mixtures to the heat release rate (HRR). Consequently, the low-temperature combustion HRR mode becomes more pronounced (from 33.9% to 76.7%) while the total HRR is reduced by a factor of 4. 3) Ignition is observed for all investigated SOI's. However, the numerical findings indicate that advancing the SOI decreases the ignition kernel size, resulting in weaker ignition. 4) An ignition index analysis with frozen flow assumption indicates that for the SOI's close to the TDC the HRR mode appears as spray mixing controlled, while for advanced SOI it becomes reactivity controlled, dominated by fuel stratification.

1. Introduction

With the increasing concern on the impact of combustion emissions on the environment, recent combustion research and new technologies are focused on mitigating high CO_2, NO_x and soot emissions. A viable solution for emission reduction is to utilize low-temperature combustion at lean mixture conditions [1]. Among these methods, Reactivity Controlled Compression Ignition (RCCI) offers a solution to NO_x-soot trade-off in conventional compression ignition (CI) engines [2]. It utilizes mixture and reactivity stratification in the combustion chamber through mixing of two (or more) fuels with different reactivities. For example, a high-reactivity fuel (HRF, e.g., diesel) is directly injected into a cylinder where the low-reactivity fuel (LRF, e.g., methane, methanol) is homogeneously mixed with the oxidizer.

RCCI may offer low emissions and control over combustion duration, strength, and phasing [3,2]. The reactivity stratification created with this method has also been proposed as a strategy to obtain more control over the ignition timing and smoother heat release rate (HRR) and combustion process, compared to e.g., Homogeneous Charge Compression Ignition (HCCI) [4]. In RCCI applications, one particular importance is the effect of injection timing on the mixture and temperature stratification and the consequent reactivity stratification, which in turn shapes the ignition characteristics. Even though RCCI offers a solution to operational issues related to other low-temperature combustion technologies such as HCCI, it may still lead to high unburned hydrocarbon (UHC) and CO emissions, which limits its operation range to medium engine loads [3,5]. In addition, the high pressure rise rates (PRR) that can be observed for certain operation conditions and injection strategies are yet to be addressed [5]. Finally, the sensitivity of the heat release rate to local perturbations in the air-fuel mixture formation may pose a challenge in controlling strategies [1].

While experimental engine tests offer a general insight on ignition characteristics, high-fidelity numerical simulations with detailed chemistry offer a more detailed understanding on the space-time

* Corresponding author.
E-mail address: bulut.tekgul@aalto.fi (B. Tekgül).

https://doi.org/10.1016/j.fuel.2021.120295
Received 17 September 2020; Received in revised form 19 December 2020; Accepted 22 January 2021
Available online 27 February 2021

dependent production and consumption of important species, as well as the low and high-temperature chemistry (LTC, HTC) and overall ignition/combustion characteristics. Direct numerical simulation (DNS) imposes a heavy computational burden and limits the investigation to simple geometries and certain simplifying assumptions. In contrast, large-eddy simulation (LES) has been shown to be a computationally feasible and predictive simulation strategy for turbulent spray combustion [6,7]. In this respect, our previous LES studies [6,8] characterized the following aspects of dual-fuel (DF) ignition, with relevance to the current study: 1) the LTC is known to be of significant importance in the DF spray ignition HRR, and 2) the amount of injected diesel quantity should be large enough to achieve stable ignition characteristics. These studies revealed ignition trends in contrast to *n*-dodecane spray in single-fuel conditions including: 1) delayed ignition of *n*-dodecane spray in a lean methane-air mixture at T = 900 K [6] due to the addition of the LRF to the ambient oxidizer and 2) delayed ignition of *n*-dodecane spray in a lean methane-air charge when the injection duration became shorter [8]. Such observations further motivate our analysis on DF spray ignition.

Fig. 1 shows the main characteristics of dual-fuel spray ignition after the onset of the high-temperature combustion. The simulation and discussion below is based on our previous studies, e.g., [6,8,9]. It is noted how the injected HRF droplets accelerate a multiphase jet which undergoes a transition to turbulence. The enhanced mixing promotes the entrainment of hot ambient gases to the spray axis, which eventually leads to rapid evaporation and termination of the liquid phase at the liquid length. As a result, a region of low temperature chemistry emerges, which is characterized by the intermediate species formed during the HRF decomposition (e.g., H_2O_2). The ignition kernels that are formed in locally reactive regions of the spray act as "chemical sparks", which then form the high temperature combustion region within the mixed HRF-LRF charge. The location, size, and strength of the ignition kernels control the subsequent high temperature heat release and depend on the local reactivity and overall stratification within the spray charge. For this reason, applications that control the mixture and reactivity of the charge through different operations and injection strategies (e.g., RCCI), may offer control over ignition and heat release rate characteristics.

Experimental studies on RCCI provide insight on ignition timing effects, combustion efficiency, and emission reduction [10–14]. In particular, Kokjohn et al. [10] showed that in RCCI type engines, it is possible to achieve certain prescribed emission targets at various load points by avoiding high equivalence ratios and high temperature regions during the combustion process. Moreover, Liu et al. [13,14] reported that in RCCI conditions, the combustion process depends on the local fuel reactivity (through concentration), which can be regulated through different injection strategies. In summary, they concluded that the heat release, ignition, and flame propagation characteristics can be substantially influenced by the chosen injection strategy.

From the numerical simulation perspective, there are a number of RANS/LES studies investigating the RCCI ignition and combustion at various conditions. In particular, Liu et al. [15,7] investigated the combustion kinetics with RANS and LES and concluded that there are four characteristic stages in RCCI combustion: 1) initial low-temperature heat release (LTHR) from the decomposition of the high-reactivity fuel and intermediate species formation, 2) intense LTHR with increase in the system temperature and formation of low-temperature combustion species such as CH_2O, 3) early high-temperature heat release (HTHR) and 4) intense HTHR with substantial heat release. In addition, Kakaee et al. [16] showed that the increase in premixed charge equivalence ratio may delay the start of combustion. Moreover, a number of DNS studies have recently analyzed the RCCI combustion in detail [17–22]. In particular, Bhagatwala et al. [22] studied different combustion modes under RCCI conditions through 1-D and 2-D DNS analysis and concluded that fuels with high-reactivity and negative-temperature coefficient (NTC) behavior tend to generate heat mainly through flame propagation, while low-reactivity fuels prefer ignition fronts. In addition, Luong et al. investigated the chemical aspects and overall properties of RCCI process [19,20], as well as the effect of injection timing on the ignition of stratified DF mixtures [21]. They reported that 1) the combustion phasing and the peak HRR can be controlled by adjusting the injection timing of the high-reactivity fuel and 2) the overall HRR is more distributed over time compared to the Stratified Charge Compression Ignition mode.

Within the RCCI context, determination of the actual combustion mode has been of particular research interest due to the different influence of deflagrative versus spontaneous propagation on emissions and combustion efficiency [23]. Several numerical [22,21,19,20,24] and experimental [25,15] investigations have observed either of the two modes of combustion under different reactivity stratification levels, with direct relevance to the injection timing as well. Recently, Karimkashi et al. [24] discussed the connection between reactivity stratification amplitude and spatial scale on the observed combustion mode. In particular, deflagrative and spontaneous combustion modes were

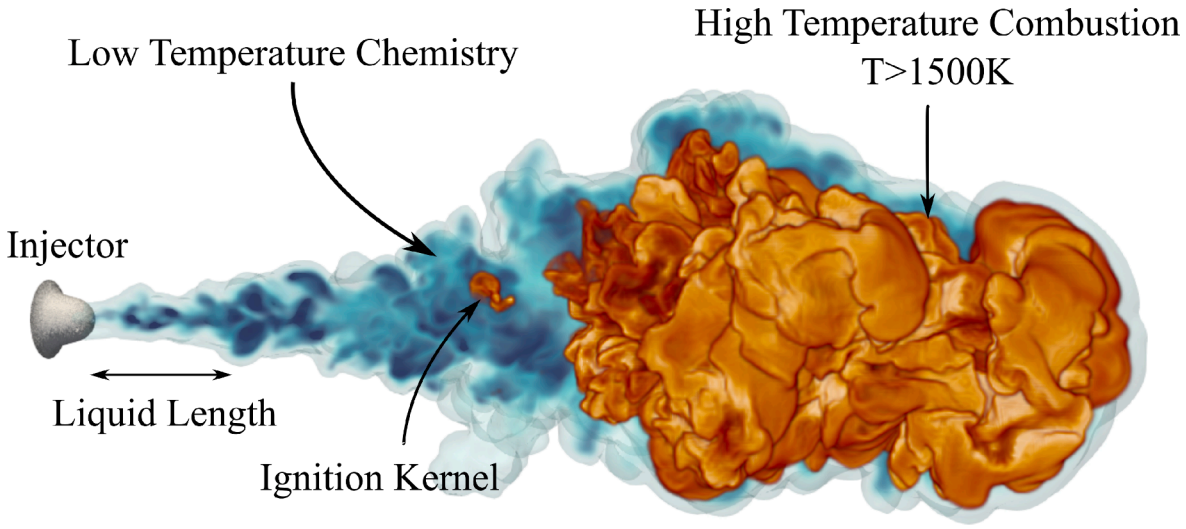

Fig. 1. A volume rendered representation based on our previous LES analysis on dual-fuel spray ignition in stationary ambient conditions [9] at a grid resolution of $\Delta = 62.5$ μm. Blue color represents low-temperature chemistry (specie H_2O_2) while red color shows high-temperature combustion ($T > 1500$ K). (For interpretation of the references to colour in this figure legend, the reader is referred to the web version of this article.)

identified and characterized via 1D/2D numerical studies and theoretical analysis with linkage to RCCI combustion. The simulations herein do not reach the deflagration phase, but they are mostly limited to spontaneous ignition in the spray region.

While several numerical studies have investigated RCCI combustion, only limited efforts have been devoted to the numerical study of fuel spray injection timing effects on the mixture and thermal stratification levels as well as ignition characteristics. In a recent study, Li et al. [26] investigated the effect of advancing the start of injection (SOI). They observed that ignition timing first advances with the SOI shifting away from the top-dead center (TDC). Then, by further advancing the SOI, the ignition timing starts to retard towards the TDC. Such a behavior may potentially enable the control of ignition timing in a short time range by adjusting the SOI. Consequently, the observed trend on the SOI has a close relevance to the present study as well.

In this work, we continue and extend our earlier numerical dual-fuel spray studies [6,8,9] in a constant volume domain with dynamic conditions. For computational feasibility, we emulate the compression heating effects relevant to engines by using a source term in the governing equations. The setup offers an academic framework suitable for high-resolution LES of diesel sprays in RCCI-like conditions without mesh motion. To our knowledge, this is the first study utilizing such an approach in LES framework, enabling the investigation of compression effects on spray-induced ignition. The utilized simplified computational setup offers 1) avoiding the complexity of moving engine geometry, 2) avoiding spray-wall interaction with high computational requirements, and 3) targeted information on the ignition characteristics. A diesel surrogate (*n*-dodecane) is injected into a homogeneous methane-oxidizer mixture as a single injection with different SOI values to investigate the influence of injection timing under compression on mixture formation and spray ignition. Additionally, in the end of the paper, we provide brief experimental evidence to support and motivate our numerical results. The objectives of the present study are:

1. Investigate the relationship between ignition characteristics and the SOI through numerical analysis. In particular, we quantify the effect of the SOI on the mixture distribution and the HRR characteristics.
2. Analyze the heat-release rate modes and contribution of low-temperature chemistry to these modes for different injection timings.
3. Quantify the mixture and reactivity stratification within the spray through an ignition index analysis.

2. Numerical methods and experimental setup

In this section, a brief summary of the utilized numerical methods and experimental setup is given. For further information regarding turbulence and combustion modeling in the OpenFOAM framework [27], the reader is referred to our previous publications [6,9].

2.1. Governing equations and discretization

The gas phase fluid flow is governed by the compressible Navier-Stokes equations. Mass conservation, momentum, species concentration, and enthalpy equations are solved in reactive flow simulations. LES formulation of these equations with Favre filtering is given as:

$$\frac{\partial \overline{\rho}}{\partial t}+\frac{\partial \overline{\rho}\widetilde{u_i}}{\partial x_i}=\overline{S}_{\rho}, \tag{1}$$

$$\frac{\partial(\overline{\rho}\widetilde{u_i})}{\partial t}+\frac{\partial\left(\overline{\rho}\widetilde{u_i}\widetilde{u_j}\right)}{\partial x_j}=\frac{\partial}{\partial x_j}\left(-\overline{p}\delta_{ij}+\overline{\rho}\widetilde{u_i}\widetilde{u_j}-\widetilde{\overline{\rho}u_iu_j}+\overline{\tau}_{ij}\right)+\overline{S}_{u_i}, \tag{2}$$

$$\frac{\partial\left(\overline{\rho}\widetilde{Y_k}\right)}{\partial t}+\frac{\partial\left(\overline{\rho}\widetilde{u_i}\widetilde{Y_k}\right)}{\partial x_i}=\frac{\partial}{\partial x_i}\left(\overline{\rho}\widetilde{u_i}\widetilde{Y_k}-\widetilde{\overline{\rho}u_iY_k}+\overline{\rho}\widetilde{D}\frac{\partial\widetilde{Y_k}}{\partial x_i}\right)+\overline{S}_{Y_k}+\overline{\dot{\omega}}_k, \tag{3}$$

$$\frac{\partial\left(\overline{\rho}\widetilde{h_t}\right)}{\partial t}+\frac{\partial\left(\overline{\rho}\widetilde{u_j}\widetilde{h_t}\right)}{\partial x_j}=\frac{\partial\overline{p}}{\partial t}+\frac{\partial}{\partial x_j}\left(\overline{\rho}\widetilde{u_j}\widetilde{h_s}-\widetilde{\overline{\rho}u_jh_s}+\frac{\overline{\lambda}}{\overline{c_p}}\frac{\partial\widetilde{h_s}}{\partial x_j}\right)+\overline{S}_h+\overline{\dot{\omega}}_h, \tag{4}$$

where $\overline{\rho},\widetilde{u_i},\overline{p},\widetilde{Y_k},\widetilde{h_s},\overline{\tau}_{ij}$ denote filtered density, velocity, pressure, mass fraction of kth species, sensible enthalpy and viscous stress sensor, respectively. In addition, overbar ($\overline{\ }$) corresponds to unweighted ensemble average and tilde ($\widetilde{\ }$) denotes density-weighted ensemble average. In energy equation (i.e., Eq. (4)), variables $\overline{c_p}$ and $\overline{\lambda}$ represent heat capacity and thermal conductivity of the mixture. Production rate of each chemical species is denoted by $\overline{\dot{\omega}}_k$ and the heat release rate (HRR) is calculated as $\overline{\dot{\omega}}_h=\sum_k\Delta h^o_{f,k}\overline{\dot{\omega}}_k$, where $h^o_{f,k}$ is the enthalpy of formation. A unity Lewis number is assumed for all species, making the diffusion coefficient $D=\lambda/(\rho c_p)$. The set of governing equations are completed by the ideal gas law and thermal equation of state.

The governing equations are discretized using the finite volume method with a second order time integration scheme. While the diffusive fluxes are discretized to yield a second order spatial accuracy, the convection terms are discretized using a second order accurate, non-linear, locally dissipative interpolation scheme called the Gamma scheme [28], similar to our previous reactive and non-reactive spray studies [29,30,6,8,9]. The pressure-velocity coupling is implemented via the PIMPLE algorithm.

2.2. Spray and combustion models

A diesel surrogate (*n*-dodecane) liquid spray is injected into the computational domain using Lagrangian Particle Tracking (LPT) method, allowing two-way coupling between two phases without inter-particle collisions. Unlike our previous work [6,8], an explicit droplet break-up modelling approach is not utilized due to the uncertainty of these models at varying ambient pressure and temperature conditions. Instead, a constant droplet diameter of 0.5 μm is used by assuming that the spray has already undergone the secondary break-up process following Kaario et al. [31], which showed good agreement with the Engine Combustion Network (ECN) Spray A experiments at baseline conditions (900 K, 60 bar). This modeling decision is further supported by validating the constant droplet size approach with the liquid and vapor penetration data provided by the ECN [32] for different density, temperature, and injection pressure points and they are presented in Fig. 2 .

A finite-rate chemistry approach with a skeletal chemical mechanism by Yao et al. [33] (54 species and 269 reactions) is utilized. The choice of the chemical mechanism is based on its relatively good performance in our previous studies with both *n*-dodecane and *n*-dodecane-methane oxidation processes [6,8,9].

In our OpenFOAM implementation, the chemical Jacobian matrix, required by the finite-rate chemistry approach, is obtained from the open-source library pyJac [34]. The stiff chemical ODE problem is solved for each computational cell, using a linearly implicit extrapolation method (Seulex) with a high-order (up to 12th) accuracy [35]. Finally, the imbalance of the computational load originating from varying the chemistry CPU load in different processors is eliminated by utilizing dynamic load balancing of the chemistry problem on the fly using Message Passing Interface (MPI) routines. In addition, a reference cell mapping approach described in [9] is used to obtain further chemistry speed-up.

The turbulence-chemistry interaction (TCI) is modeled through a first-order closure assumption and no explicit subgrid scale model is applied to Eqns. (3) and (4). Following our previous work [6,8,9], it is assumed that the fine mesh resolution ($\Delta=62.5\,\mu m$) together with the intense spray mixing enables finite-rate chemistry approach to predict the ignition characteristics accurately. In addition, the focus of this study is targeted to the spray autoignition process, which is assumed to

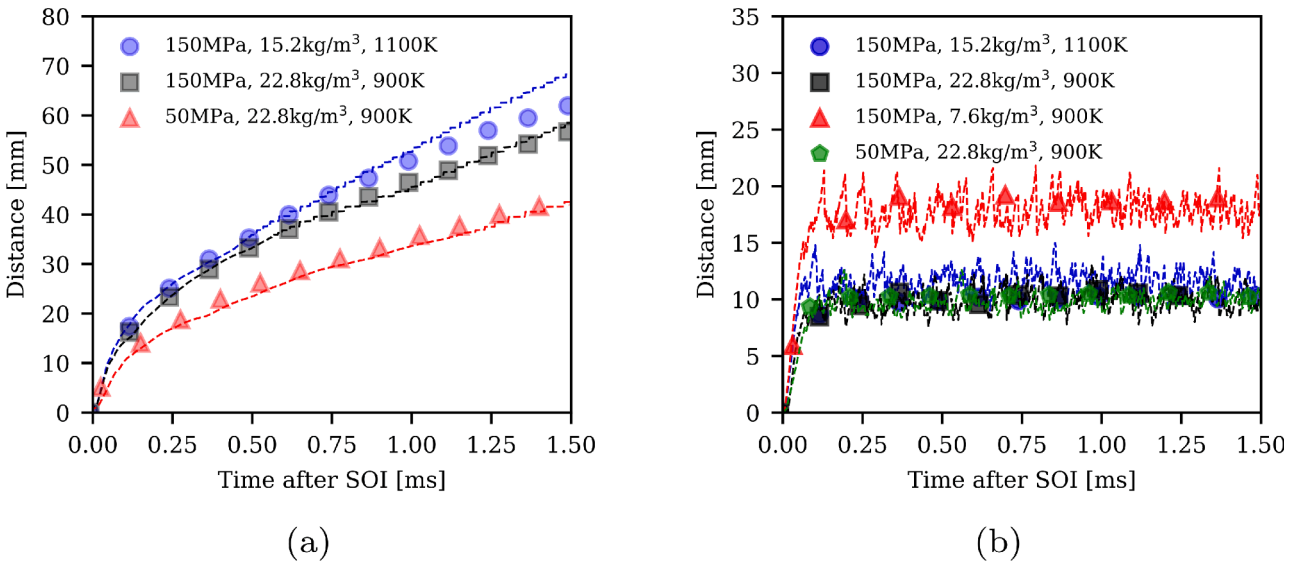

Fig. 2. Comparison of (a) vapor and (b) liquid penetration for various ECN Spray A conditions between the simulations (dashed line) and experiments (symbol). It is noted that under stationary conditions without compression, the no-breakup model approach provides good agreement with the global spray metrics which are commonly known to be important in determining spray ignition location and timing.

be less sensitive to micro-mixing issues [36], compared to e.g., quasi-steady flame lift-off length estimation in the ECN Spray A context [37]. Furthermore, our comparison of the current no-model approach with a flamelet-generated manifold method using a presumed PDF approach indicated an ignition delay time (IDT) difference around 1% [6]. It is also important to point out that all results presented here focus on the spray ignition region before any actual flame formation within the premixed charge without existence of the injected spray, where the TCI model is required.

2.3. Compression heating model and case setup

For the numerical analysis, a cylindrical domain with 108 × 108 mm dimensions is used, similar to ECN experimental vessel [32] and previous studies [30,38,39]. In RCCI conditions, the direct injection of the high-reactivity fuel may occur earlier during the compression stroke (¯50 CAD BTDC) [2]. Hence, the influence of volumetric compression must be considered in order to account for the evolution of thermo-physical properties (i.e., pressure and temperature) correctly. In contrast, in dual-fuel engines which utilize pilot injection systems the spray injection is quite close to the top dead center (TDC), allowing the use of constant thermophysical conditions in experimental and numerical analyses [6,9]. As shown in the recent literature, the compression heating effect can be modeled by additional mass and energy source terms in the governing equations [40,22,21]. Following the formulation presented in [21,40], a compression heating model is utilized to mimic a motored pressure trace and the subsequent temperature rise, while the pressure rise due to the combustion event itself is neglected. We let the local pressure rise originating from combustion to evolve on its own, following the approach adopted by [21].

According to the kinematic equations for piston motion, the motored pressure of an engine cylinder near the TDC can be approximated using:

$$P_m(t) = P_{0,m}\left[1 + g^2\pi^2\frac{t - t_0^2}{t_c^2}\right]^{-n}, \tag{5}$$

$$\dot{m} = \frac{\rho}{P}\frac{dP_m}{dt}, \tag{6}$$

where $P_{0,m}$ is the desired motored pressure value at the TDC, t_c is the time it takes for one crank rotation, t_0 is the time at the TDC point and g and n are model constants for matching the engine geometry. The mass source term $\dot{m}$ is then added to the right hand side of all governing equations to follow the desired pressure curve. A schematic describing the constant volume numerical setup is given in Fig. 3.

An engine compression curve (see [41]) is calculated in Cantera [42] and compared with the compression heating model described in Eqs. (5–6), presented in Fig. 4. Here, the TDC conditions were chosen to correspond to the ECN Spray A conditions [32], in which our previous numerical DF studies were also carried out [6,8]. Here, a 500 bar injection pressure was used, as validated against the ECN data in our previous publication [30]. In total, five different cases are selected to investigate the influence of the SOI on ignition characteristics. Details of the simulation setup and investigated conditions are provided in Tables 1 and 2. A constant grid size of 62.5 μm is used throughout the region where the spray penetrates. The mesh resolution is assumed adequate for the present study within the bounds of analysis details presented later, based on various previous studies showing good agreement between LES and experiments under non-reacting [43] and reacting [29,30,6,9,44] conditions with the same resolution.

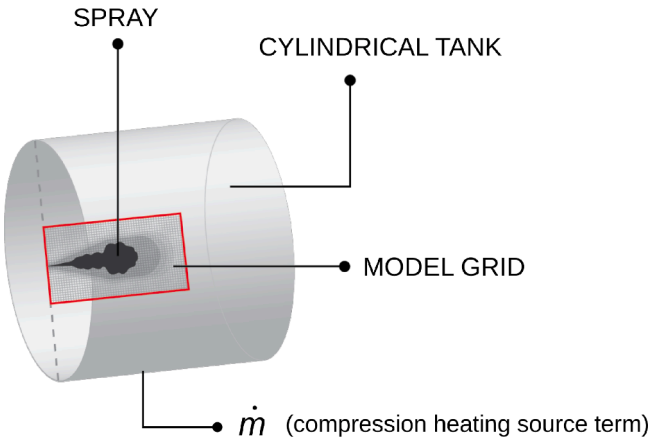

Fig. 3. A schematic of the numerical setup used in the simulations. The spray is injected into a constant volume vessel, while the compression effects are simulated through a source-term approach without mesh motion.

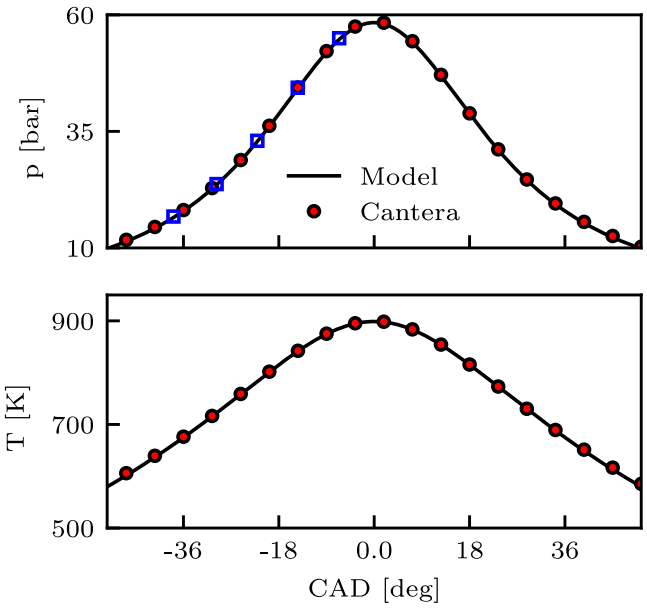

Fig. 4. Comparison of motored pressure and corresponding temperature curves between the present implementation (—) and Cantera (●). The SOIs are denoted by (□) (see Table 2).

Table 1
Simulation configurations.

Engine and injection parameters	
Compression ratio	*16:1*
Engine speed	1200 RPM (7.2 CAD = 1 ms)
T_{TDC}	900 K
p_{TDC}	60 bar
SOI	−7.2 to −36 CAD
Injection duration	3.6 CAD (0.5 ms)
Injection pressure	500 bar
Conditions for ambient charge	
Initial CA	−36 CAD
Initial mean temperature	663 K
Initial mean pressure	17 bar
X_{O_2}	0.15
X_{CO_2}	0.05955
X_{H_2O}	0.0346
X_{N_2}	0.71835
X_{CH_4}	0.0375
ϕ_{CH_4}	0.5
Z_{st} (Stoichiometric mixture fraction)	0.0234

Table 2
Investigated cases with different SOI timings.

Initial conditions	SOI-7.2	SOI-14.4	SOI-21.6	SOI-28.8	SOI-36
t_{SOI} [CAD BTDC]	7.2	14.4	21.6	28.8	36
T_{SOI} [K]	886	842	784	723	663
p_{SOI} [bar]	53.6	43.6	32.7	23.7	17.0

2.4. Experimental setup

The experimental results have been obtained from a single-cylinder laboratory engine, also utilized in our previous studies [45,8]. The primary fuel (pure CH_4) is port-injected and the diesel-fuel is directly injected from a common rail 3-hole (160 μm) piezo injector with 100 MPa rail pressure. Following our simulation configuration, the engine speed was set to 1200 RPM and the target equivalence ratio, chamber pressure and charge temperature at the TDC are estimated to be ϕ_{CH_4}=0.5, 60 bar and 900 K respectively, assuming isentropic compression.

The laboratory engine is based on an AGCO 84 AWI 6-cylinder common rail diesel engine and it is converted into a single-cylinder configuration, providing control over the fuel injection system, intake air, valve actuation and exhaust. A methane port injection system was adopted for distributing methane into the intake manifold at 360 CAD BTDC during the intake stroke. The pilot diesel fuel SOI is advanced from 5 to 75 CAD BTDC with t_{inj} = 0.242 ms (≈ 2.45 CAD).The combustion process is monitored by measuring the in-cylinder pressure trace using a Kistler pressure transducer mounted in the cylinder head. The pressure data was sampled every 0.2 CAD and it was further processed to calculate the net HRR.

3. Results and discussion

In Conventional Diesel Combustion (CDC), the injection of the HRF is close to TDC and the combustion characteristics are controlled by the mixing rate of the fuel with the ambient charge. In contrast, RCCI aims to obtain a reactivity stratification within the fuel charge through different (e.g., earlier) injection strategies and provide control over the ignition and HRR characteristics with a leaner charge and mixture stratification. The following results utilize these two concepts and the transition in between them with different SOI timings.

3.1. Ignition timescales

First, the effect of the SOI on ignition timing is investigated. Fig. 5 shows the first (τ_1) and second stage (τ_2) ignition delay time (IDT) for different SOI values. The IDT values are presented with respect to both the top-dead center (TDC) (in CAD) and the SOI (in ms). Here, τ_1 is defined as the time instance when 20% of the maximum dodecyl peroxy radical $C_{12}H_{25}O_2$ (RO_2) concentration is reached, while τ_2 is defined as the time instance when the local consumption of the available ambient CH_4 exceeds 95% in any computational cell, consistent with our previous work [8].

As seen in Fig. 5 (top), advancing SOI from 7.2 to 21.6 CAD BTDC advances both τ_1 and τ_2 with respect to the TDC. The first stage ignition timing τ_1 advances from 3.2 to 10.7 CAD BTDC while τ_2 advances from 0.91 to 7.08 CAD BTDC with advanced SOI. However, with further advanced SOI from 21.6 to 36 CAD, while τ_1 advances further to 12.25 CAD BTDC, τ_2 starts retarding towards the TDC to 4.46 CAD BTDC, caused by lower reactivity of the spray charge due to over-dilution and a subsequent shift in ignition timing characteristics. This shift is related to the change of combustion mode from mixing controlled, resembling the CDC, to reactivity-controlled. This observation supports the findings of Li et al. [26], where they observed ignition to first advance and then retard with advancing SOI relative to the TDC. In addition, it can be observed that while τ_1 does not exhibit the same non-linear behavior with respect to the TDC, its rate of change decreases when SOI is further advanced.

When the ignition time is defined with respect to the SOI (Fig. 5, bottom), it can be seen that with an earlier SOI, both τ_1 (0.56 to 3.30 ms) and τ_2 (0.87 to 4.38 ms) advance. Such a behavior is expected since as SOI is advanced, the initial temperature and pressure of the ambient charge both decrease (Table 2), reducing the overall reactivity. It is also worth noting that while τ_1 and τ_2 both increase with advanced SOI, the chemical induction time between the two timescales (τ_2 - τ_1) is less affected. This is consistent with our previous observations on ignition characteristics at different ambient temperatures [9]. In summary, the findings of this subsection indicate that the main ignition (τ_2) depends non-linearly on SOI with respect to the TDC. While τ_2 first advances away from the TDC with advanced SOI, after a critical point τ_2 retards towards the TDC due to the very early injection and subsequent over-dilution.

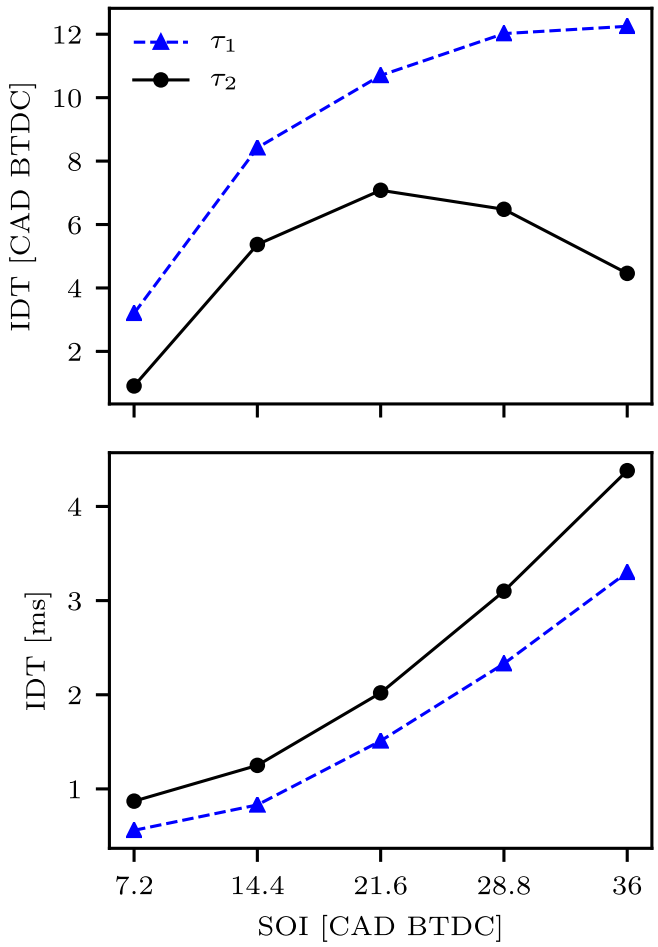

Fig. 5. First and second stage ignition (τ_1, τ_2) times obtained from the 5 simulations with varying SOI. Timing with respect to the TDC in CAD (top) and the SOI in ms (bottom) are presented respectively. The ignition timing advances with advanced SOI, then it starts to retard towards the TDC after a critical point.

3.2. Mixing and chemistry

Next, the mixture formation and subsequent ignition kernel characteristics of the different SOI timings are investigated. The mixture conditions, in which ignition is initiated, control the ignition kernel structure and subsequent kernel propagation in the lean methane-air charge. Advancing the SOI creates an overall leaner spray mixture, which helps in reducing NO_x and soot emissions. The size and location of the formed ignition kernel is also an important parameter to ensure a robust ignition to be followed by the successful consumption of the low-reactivity fuel-air mixture. To investigate the mixing characteristics and ignition kernel formation, cutplanes of various fields obtained from cases SOI-7.2, 21.6 and 36 are presented in Fig. 6 at their corresponding τ_2+0.2 ms time instances. The change in mixture characteristics and ignition strength is clearly observed: for SOI closer to the TDC at 7.2 CAD (left), most of the mixture is above stoichiometry due to the short mixing time. Due to the rich conditions associated with the short mixing time, the high-temperature ignition kernel is large in volume and forms a robust energy source for the subsequent propagation into the ambient charge. The specie H_2O_2associated with the low-temperature chemistry (LTC), is fully consumed within the rich spray charge, indicating that the shift from the LTC and the high-temperature chemistry (HTC) regime is already underway within this region. Finally, the ambient CH_4 within the spray charge is almost fully consumed, further showing that the ignition is strong and already locally consuming the ambient fuel.

By advancing the SOI to 21.6 CAD (middle) and even further to 36 CAD (right), we observe that the fractional spray volume that is above stoichiometry gets smaller with advanced SOI. In addition, the ignition kernels formed within the rich regions get smaller in volume with advanced SOI. For the SOI-21.6, the high-temperature ignition kernel still exists inside the rich spray regions, now smaller in volume, while both the rich and lean portions of the spray still contain H_2O_2 and CH_4, indicating the LTC. Similarly, for the SOI-36 case the ignition kernels are confined to the rich region at the tip of the spray charge, whereas majority of the spray is lean. The lean region with H_2O_2 is more widespread in space, indicating a larger LTC region.

Conditional means and scatter data distributions of H_2O_2, CH_4, temperature and the HRR in Z space are presented in Fig. 7. The data is presented at the same time instances with Fig. 6 to enable a direct comparison. First, it is noted that the ignition and overall heat release occur further away from the injector with advanced SOI. The color of the scatter data shows that while for the SOI-7.2 CAD ignition is closer to the injector between 20 to 30 mm, for the SOI-21.6 the location shifts to ~40 mm and for the SOI-36 reactivity at >50 mm is observed. Although not visible here, local spatial stratification also exists for each case within their respective reactive region.

Based on Fig. 7, a few observations can be made. First, it can be seen that the SOI-7.2 case spans a broader range of mixture fraction conditions in comparison to the other two cases. Although the conditional mean of the HRR spans around stoichiometry, data points between $0.05< Z <0.09$ indicate a very low HRR conditional mean and the existence of CH_4 at these mixture conditions, showing reactivity in these rich conditions. It can be inferred that an ignition kernel forming at these rich conditions would lead to higher burning temperatures and emissions. For advanced SOI, it can be seen that the data points are on a narrower band in the mixture fraction space and distributed around/below stoichiometry. In addition, the conditional mean of H_2O_2 gets larger, indicating a stronger low-temperature combustion. Finally, the overall shift to leaner conditions indicates an overall low-temperature and lean HRR, which is analyzed in detail in the following subsection. In summary, the findings here show that with advanced SOI the spray charge gets leaner, posing a larger volumetric extent of the LTC region. Consequently, the high temperature ignition kernel is formed more downstream and it is smaller in volume due to the leaner charge and a lower growth rate.

3.3. Heat release rate

The evolution of the HRR as a function of SOI is provided in Fig. 8 for the SOI- 7.2, 21.6, and 36 cases. On the logarithmic scale, two peaks in the HRR are observed. The peaks correspond to the low-temperature heat release rate (LTHR) and high-temperature heat release rate (HTHR). We note that the peak HRR value at the time of ignition decreases with advancing the SOI and this behaviour is most visible for the SOI-36 case, where the LTHR is less dominant, and the HTHR is around 40% smaller than the SOI 7.2 case. It can be seen from the figure that while for the SOI-7.2 and 21.6 cases the HRR has distinct peaks for the LTHR and HTHR, for the SOI-36 case a more flat HRR distribution between τ_1 and τ_2 is observed. For this case, a large volume of the spray charge releases heat below stoichiometry in the LTC regime as a result of the long mixing time (see Fig. 6). These regions have high LTC species concentrations but low temperature values, resulting in lower HRR per unit volume and the flat profile. The details of different HRR modes as a function of SOI are described in the following.

To study the relationship between the SOI and the HRR modes, Fig. 9 shows a volume integrated total HRR, conditioned with pre-defined combustion modes, c.f. Table 3. In detail, the affiliation between the combustion modes and the total HRR is the following:

- LTC: early decomposition of *n*-dodecane into RO_2.
- Late-LTC: accumulation of species related to LTC, such as RO_2, H_2O_2 and CH_2O.

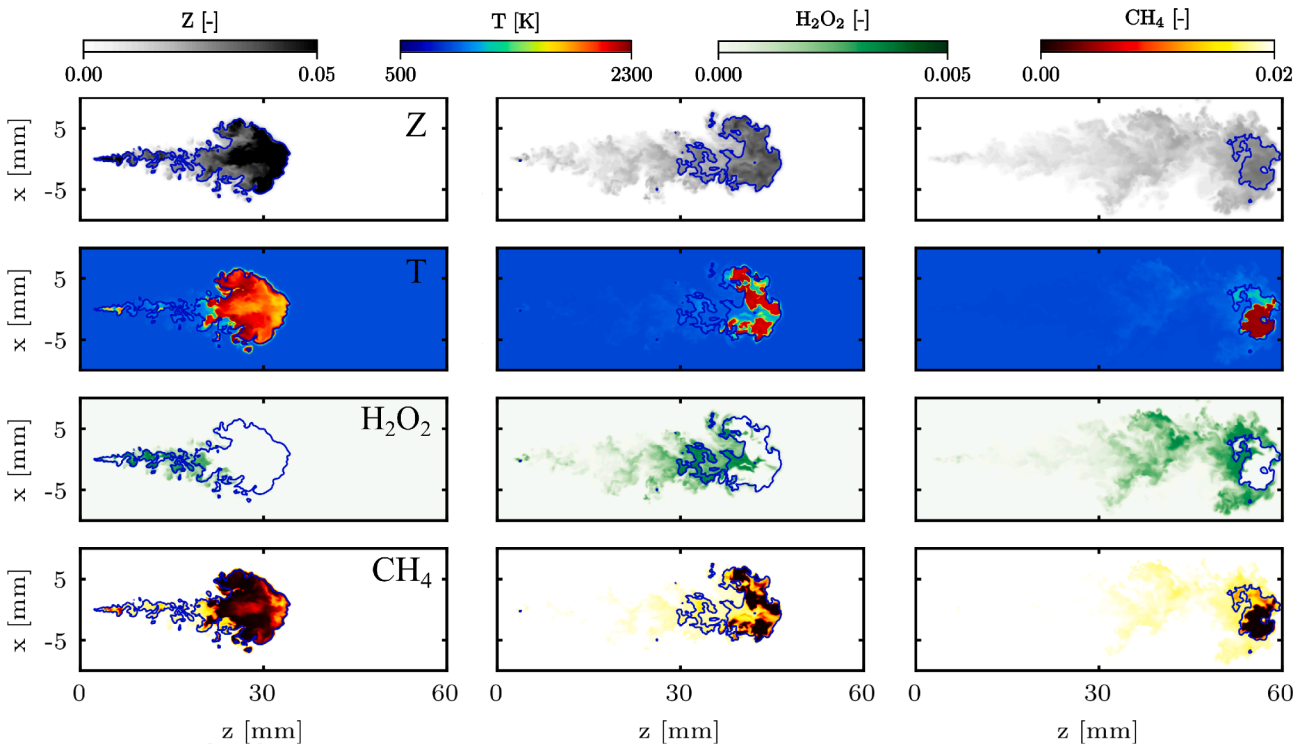

Fig. 6. Mixture fraction, temperature, H_2O_2 and CH_4 cutplanes for cases SOI- 7.2 (left), 21.6 (middle) and 36 (right), at their corresponding IDT+0.2 ms time instances (blue isoline represents Z_{st}). The lower reactivity due to overdilution and subsequent downstream shift in ignition kernel location and reduction in its size can be observed. (For interpretation of the references to colour in this figure legend, the reader is referred to the web version of this article.)

- Pre-HTC: low T values but high LTC species concentration, prior the HTC.
- HTC-pre-ign.: high T values but no HTC related species (OH) present.
- HTC: high T values and high OH concentration.

The first 3 modes (LTC, Late-LTC, and Pre-HTC) represent the low temperature combustion contribution and the subsequent LTHR, while the last 2 modes (HTC-pre-ign. and HTC) describe the high temperature combustion and HTHR. The species threshold values used in determining the combustion modes were selected based on 0D homogeneous reactor analysis and available LES data, similar to [8,46]. In addition, the chemistry modes were found to be insensitive to the threshold values for the selected order of magnitudes. The decomposition of the total HRR into the modes (see Table 3) is presented in Fig. 9 for different SOI, where the hatch pattern is also used to denote rich mixture conditions.

First, for the SOI-7.2 case (top), the peak HRR is approximately 3-4 times larger compared to the SOI-21.6 (middle) and the SOI-36 CAD (bottom) cases. In addition, the source of the HRR is exclusively concentrated in the rich conditions. It can also be seen that the Pre-HTC region, which represents the transition from low to high temperature combustion, accounts for a very small amount of the total HRR, explaining the distinct two-stage HRR structure observed in Fig. 8. The HRR follows a structure similar to CDC, mainly due to the SOI very close to the TDC. For this case, the contribution of the LTC (LTC, Late-LTC and Pre-HTC modes) to the overall HRR is 33.9 %.

Furthermore, in Fig. 9, for the SOI-21.6 case (middle), similar characteristics to the SOI-7.2 case are observed. The HRR occurs mostly at richer conditions except for a small percentage of lean contribution at Late-LTC and Pre-HTC modes. However, it can be seen that the HTC-pre-ign. mode is narrower and HTC has an overall lower contribution to the HRR. The contribution of the LTC to overall HRR is 63.5 %, almost 2 times larger than SOI-7.2. Finally, with further advancing SOI (bottom), it can be seen that lean conditions start to be the dominant HRR source. A substantial increase in the relative contribution of the Pre-HTC mode can be observed (56.0 %), which is associated with the low temperature chemistry originated HRR. Such an observation explains the steady HRR profile observed for SOI-36 case in Fig. 8. Finally, the contribution of the LTC modes increases up to 76.7 %, indicating a low-temperature chemistry dominated ignition structure. It is also important to note that the RCCI ignition follows a similar 4-stage structure to the one explained in Section 1, as discussed in Ref. [15]. In summary, the numerical observations in this subsection indicate that with advancing SOI, the peak HRR drops considerably due to the longer mixing time and the subsequent leaner mixture. In addition, the contribution of low-temperature combustion (i.e., modes LTC, Late-LTC, and Pre-HTC) to spray ignition becomes more dominant compared to the contribution from high-temperature combustion (modes HTC-pre-ign. and HTC).

3.4. Reactivity stratification PDF analysis

In the previous subsections, the analysis on SOI timing effects mainly focused on the characteristics of the injected spray as “ignition source”, rather than “reactivity stratification source”. The actual difference between the two is further explored in the following. As shown in the previous subsections, advancing the SOI beyond a critical limit makes the mixture over-diluted and it prolongs the ignition timing, which may also explain the non-monotonic ignition time-SOI behavior. The diluted spray, e.g., in SOI-36 CAD case, is expected to present an interesting candidate for the stratification source. Here, we investigate the mixing, temperature, and reactivity stratification of the three case studies with different SOIs.

In order to assess the reactivity stratification in each case, a frozen-flow ignition delay time analysis is performed investigating how an evolved spray envelope would ignite under a frozen flow assumption, similar to our previous work [8]. The analysis is carried out by selecting all spray cloud data points ($Z \geqslant 1e^{-4}$) from the 3D fields, obtained from SOI- 7.2, 21.6 and 36 cases at their corresponding IDT-0.15 ms time. Then, all the thermophysical information on chemistry (T, p, Y_i) is

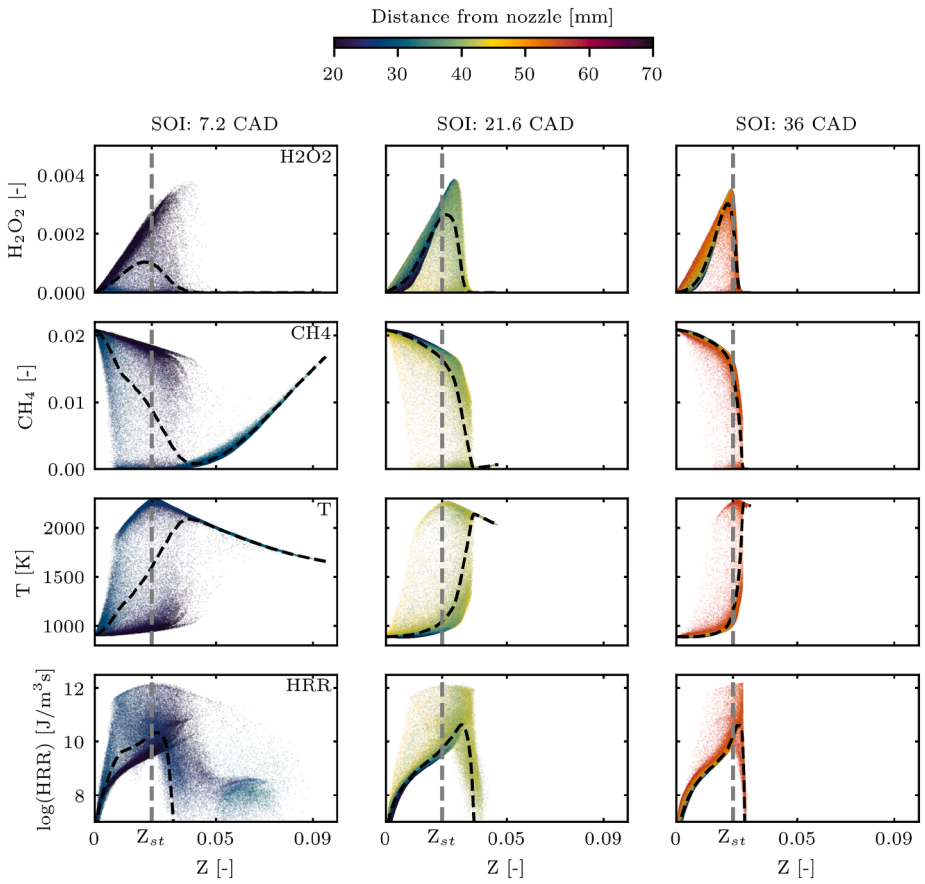

Fig. 7. Scatter distribution and conditional mean (dashed line) of H_2O_2, CH_4, temperature and HRR per unit volume in mixture fraction space for different SOI, at their corresponding IDT+0.2 ms time instances. The scatter data color denotes the axial distance from the nozzle. Note: only 2% of the 3D LES data is used for background scatter by random sampling. (For interpretation of the references to colour in this figure legend, the reader is referred to the web version of this article.)

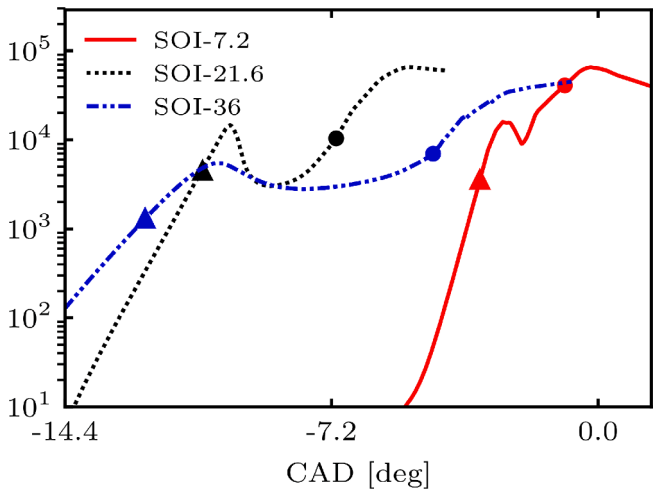

Fig. 8. Evolution of the HRR for different SOI timings. τ_1 and τ_2 are marked with (▲) and (●), respectively. It is seen that with advanced SOI the HRR has a lower peak and more flat distribution. (Note the logarithmic y-axis.)

transferred to a 0-D homogeneous reactor framework and simulations are performed under the frozen flow assumption. IDT_{0D} values obtained from these simulations reflect the reactivity of each data point at the provided initial condition. It should be noted that in this analysis the turbulent strain is neglected and the results give information solely on thermochemical characteristics inside the spray. The results presented here do not make any generalizations about the spray reactivity in non-frozen flow conditions, except for correlating and complementing the spray ignition characteristics as a function of SOI.

The probability density functions (PDF) of the 3 cases are provided in Fig. 10. The PDF analysis of the IDT_{0D} data (top) indicates that while for the SOI-7.2 case the overall reactivity is high (small IDT_{0D} values) and homogeneous (high peak in PDF), the reactivity decreases and becomes more stratified by advancing the SOI, i.e., a visible peak disappears for the SOI-36 case. Such a reactivity stratification could result from thermal or mixing heterogeneity. The temperature PDF analysis (middle) shows that initial temperature in the SOI-36 case has a distinct peak around 880 K. The reduced thermal stratification in the SOI-36 case is expected since advancing the SOI leads to more homogeneous temperature distribution levels around the ignition time. While the temperature is clustered around a certain range for the SOI-36 case, it can also be seen that the mixture fraction (bottom) is quite stratified around the lean/stoichiometric conditions with a visible peak at conditions below Z_{st}, consistent with the stratification of intermediate species in Fig. 7. The distribution of mixture fraction at lean conditions may be the cause of reactivity stratification for the SOI-36 case, since the reactivity is more sensitive to mixture fraction values at leaner conditions.

In order to give further insight on the individual effects of mixture and thermal stratification on reactivity stratification within the investigated SOI conditions, 2D binned statistics of IDT_{0D} in Z-T space is presented in Fig. 11, based on the 3D spray data. The color represents the mean IDT_{0D} value of the data points at a given Z-T bin. The following observations are noted:

- For the SOI-7.2 case (top), the majority of the mixture is above Z_{st}. The only observable reactivity stratification is noted at lower

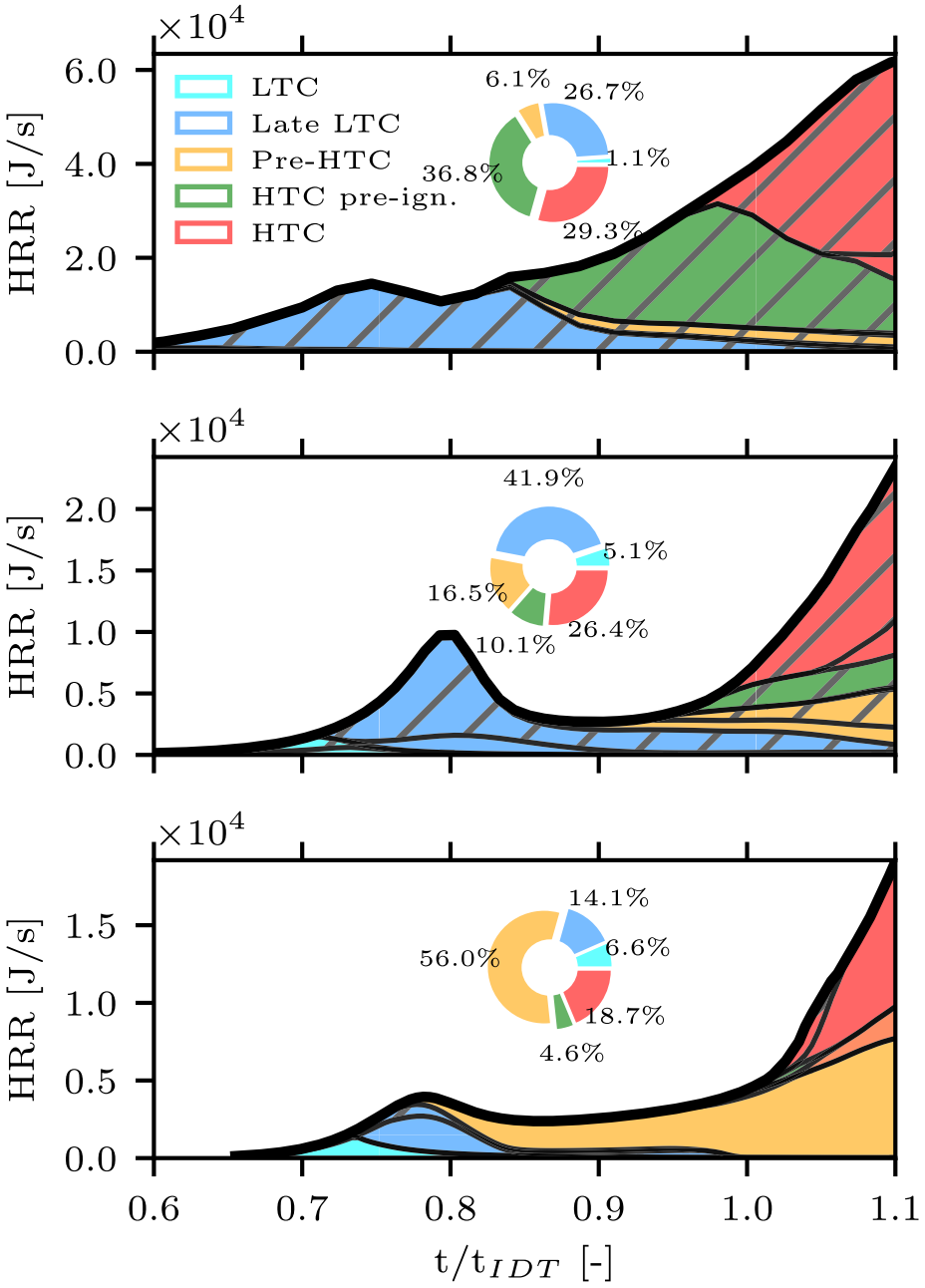

Fig. 9. Volume integrated HRR of the diesel spray ($Z \geqslant 1 \cdot 10^{-4}$) as a function of time normalized with τ_2 for the SOI- 7.2 (top), 21.6 (middle) and 36 (bottom) cases. Contribution of different chemistry modes (Table 3) to heat release as percentages is presented. The hatch pattern denotes rich mixture conditions. It is seen that the HTC modes and rich mixtures become less dominant with advanced SOI.

Table 3
HRR modes according to the underlying chemistry. ($RO_{2crit} = 1{\cdot}10^{-5}$, $H_2O_{2crit} = 1{\cdot}10^{-4}$, $OH_{crit} = 1{\cdot}10^{-5}$, $T_{crit} = 1150$K [8]).

Chemistry Mode	Definition
LTC	$(RO_2 \geqslant 1{\cdot}10^{-7}) \cap (H_2O_2 < H_2O_{2crit}) \cap (T < T_{crit})$
Late-LTC	$(RO_2 \geqslant RO_{2crit}) \cap (H_2O_2 \geqslant H_2O_{2crit}) \cap (T < T_{crit})$
Pre-HTC	$(RO_2 < RO_{2crit}) \cap (H_2O_2 \geqslant H_2O_{2crit}) \cap (T < T_{crit})$
HTC-pre-ign.	$(OH < OH_{crit}) \cap (T \geqslant T_{crit})$
HTC	$(OH \geqslant OH_{crit}) \cap (T \geqslant T_{crit})$

temperature conditions around 800 K. It can be seen that the gradient of the IDT_{0D} points in the upward direction, which indicates that the thermal stratification is the major contributor to reactivity stratification. The situation closely resembles classical diesel spray or dual-fuel pilot spray ignition conditions characterized by the $T-Z$ correspondence along the mixing line.

- For the SOI-21.6 case (middle), the mixture is confined to a narrower band in T-Z space, in the vicinity of Z_{st}. It can be seen that while the IDT_{0D} gradient is still highly biased with the T-axis, a subtle orientation towards the Z direction emerges, especially below Z_{st}.
- For the SOI-36 case (bottom), the majority of the mixture is below Z_{st}. The IDT_{0D} gradient becomes highly aligned with the Z-axis. Such an observation indicates that at lean mixtures reactivity stratification is dominantly affected by the small changes in mixture fraction rather than thermal stratification.

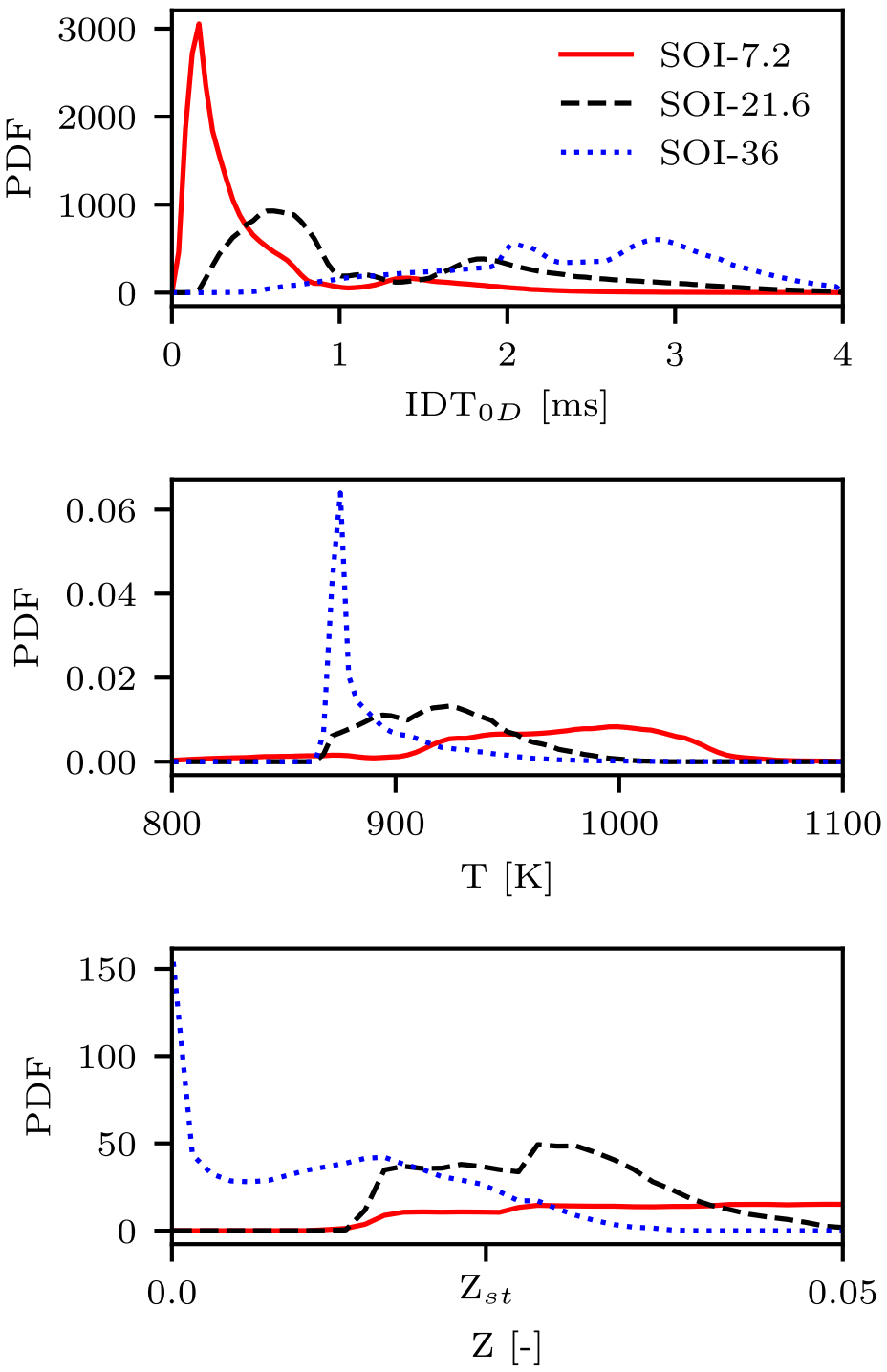

Fig. 10. PDF distribution of IDT_{0D} (top), temperature (middle) and mixture fraction (bottom) for the SOI- 7.2, 21.6 and 36 cases. Here, the statistics only consider data points within the spray envelope with relevant reactivity, i.e., $(Z > 1{\cdot}10^{-4}) \cap (IDT_{0D} < 4$ ms).

3.5. Remarks on 0d mixtures

Autoignition characteristics of different mixture conditions along the adiabatic mixing line between a fuel (*n*-dodecane) and oxidizer (CH_4+oxidizer) at different ambient temperatures is presented in Fig. 12. The location of the most reactive mixture fraction (Z_{MR}) [47] is marked in the figure by the symbols. As discussed earlier, advanced SOI results in a leaner spray, lowering the overall reactivity of the spray charge. However, advancing SOI more than a critical limit may over-dilute the spray, resulting in mixture fractions below Z_{st}, c.f. Figs. 7 and 11. Fig. 12 shows that while the overall reactivity is higher for richer mixtures (I), it is drastically lower for lean mixtures with a sharp gradient (II and III). In such lean regions, the gradients of ignition delay time (and overall reactivity) are high and susceptible to small changes in the mixture fraction, i.e., larger reactivity stratification in the mixture fraction space. In summary, the remarks above on 0D simulations illustrate the emergence of a reactivity stratified mode, dominated by fuel stratification, for lean mixtures. Such a mode is interesting due to the vastly different chemical reactivity with certain opportunities for combustion control strategies.

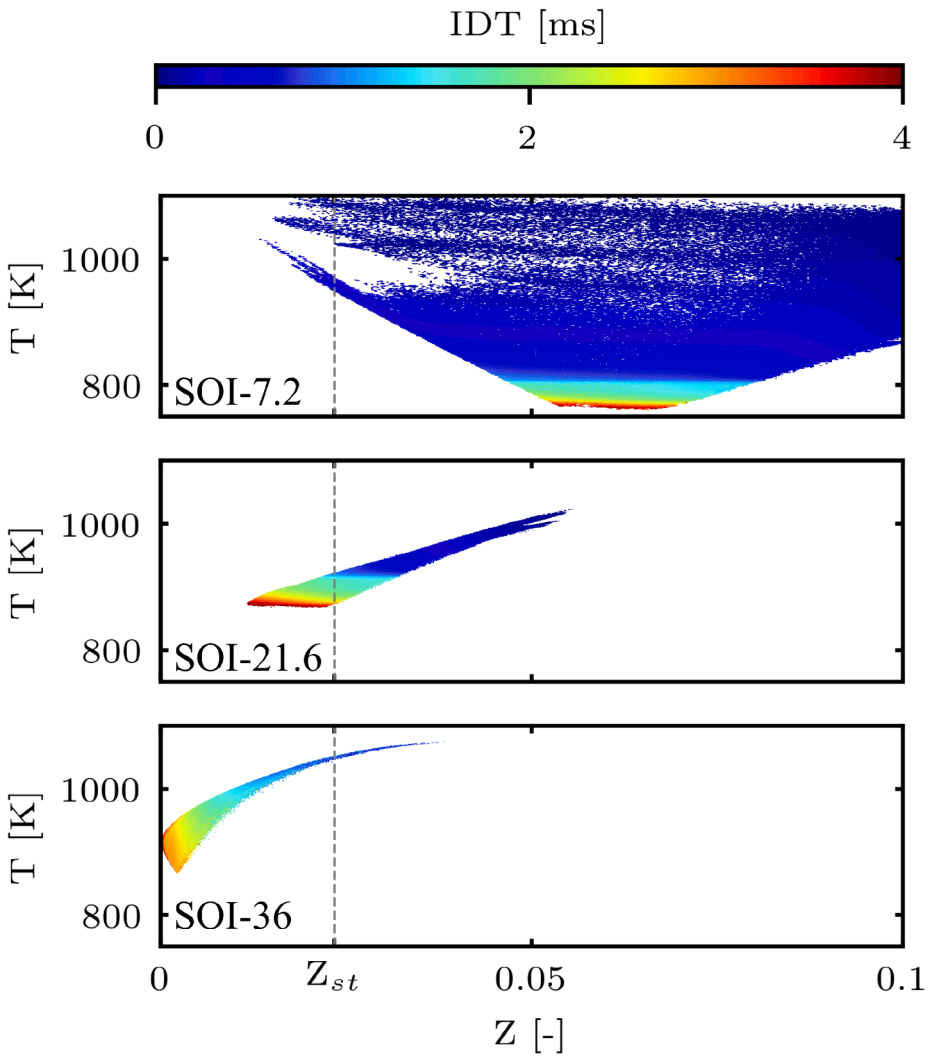

Fig. 11. Two-dimensional binned statistics of IDT_{0D} in *T-Z* space For the SOI-7.2, 21.6 and 36 cases at IDT-0.15 ms. The analysis is based on the frozen flow assumption. Contour colors represent the mean IDT_{0D} value of data points inside each bin. Reactivity stratification shifts from thermal origin (top) towards of mixture fraction biased origin (bottom) when advancing the SOI.

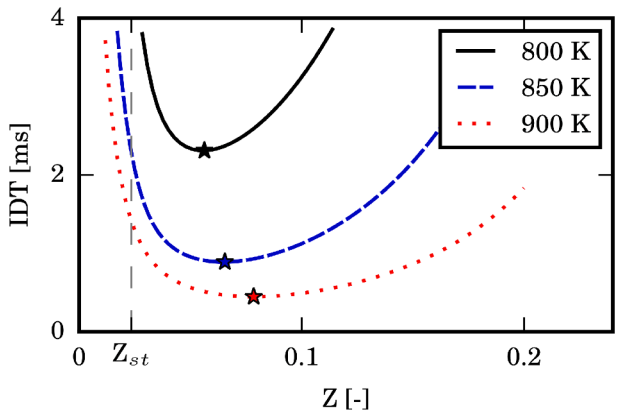

Fig. 12. Autoignition of *n*-dodecane+CH_4 at different mixture fraction conditions. The conditions are sampled from an adiabatic mixing line between pure *n*-dodecane port at 363 K and an oxidizer port with CH_4+oxidizer at varying temperatures. Z_{MR} of each case is marked with the ☆ symbol. It is seen that the reactivity gradient increases strongly when going from richer (I) towards leaner (III) mixtures with relevance to advanced ignition timings in present 3D LES and engine experiments.

3.6. Remarks on engine experiments

The main focus of the paper is the numerical modeling of the compression ignition process. However, to support the results, we also provide some experimental data in order to demonstrate the existence of the discussed phenomena. A series of engine experiments have been performed to investigate the relationship between ignition timing and SOI (for experimental setup specifications, see Section 2.4). Fig. 13a shows the mean in-cylinder pressure traces and the corresponding HRR for five different injection timings averaged over 100 consecutive engine cycles. As seen from the pressure curves, advancing the SOI first advances the ignition timing, then delays it closer to the TDC. To illustrate the effect more clearly, the ignition time as a function of SOI is presented in Fig. 13b. Here, the ignition time is defined as the time instance where 2% of the cumulative heat release is obtained. It can be seen that the ignition time advances with SOI until 35 CAD BTDC in a mixing controlled (i.e., CDC) fashion. After 35 CAD, the combustion character is noted to change. Such a "switching point" can be discussed in relation to our 3D numerical data. Based on such data, the switching point may separate two different combustion modes from one another 1) mixing controlled (rich mixtures, thermal origin) and 2) HRF mixture fraction controlled (lean mixtures). In the mixing controlled mode, ignition time advances with SOI due to the increased mixing time of the fuel-oxidizer

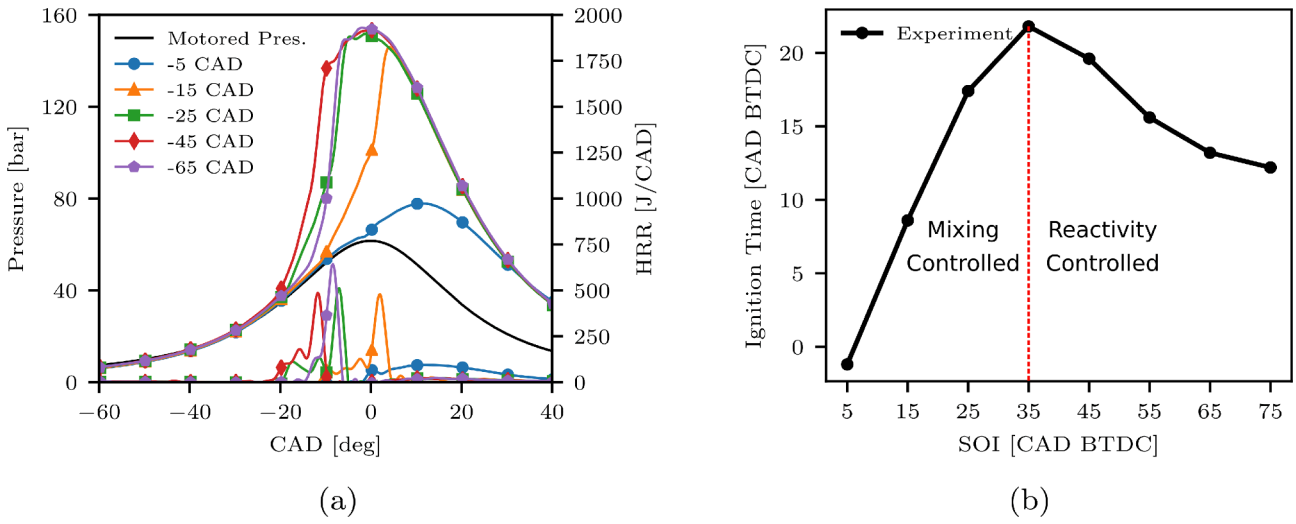

Fig. 13. (a) Mean in-cylinder pressure and net heat release rate as a function of SOI. (b) Engine ignition time values corresponding to their respective SOI's.

mixture with the advanced SOI. In contrast, in the latter mode mixing timescales are too long. Thus, ignition is dominantly controlled by the local reactivity of the diesel-methane mixture. It is important to mention that the numerical framework we use to analyze RCCI ignition does not take some factors that exist in an actual engine configuration into account, such as in-cylinder flow due to compression, heat losses and flame-wall impingement. The comparison between experimental results and our simulations are therefore limited to ignition timing, which is controlled by the reactivity of the high and low reactivity fuel mixture.

4. Discussion and conclusions

In this study, large-eddy simulation with finite-rate chemistry is used to investigate the effect of the SOI on the ignition characteristics of sprays in RCCI-like conditions. From the modeling perspective, a key challenge is to find a balance between the computational cost of the simulations and achieving a modeling setup complexity sufficient enough to make deductions applicable to the real engine context. To resolve this issue, a compression heating model is utilized to take the pressure and temperature rise into account and the effect of SOI on ignition characteristics is investigated. It was shown that the non-monotonic ignition time-SOI relationship observed in the experiments originates from over-leaning of the injected spray charge beyond a critical point with advanced SOI, where the overall reactivity has a sharper gradient. Furthermore, the effect of SOI on ignition kernel size has been investigated, which may cause cycle-to-cycle variations for advanced SOI conditions at certain operating conditions. Main findings of the study are listed in the following.

1. Advancing the SOI from 7.2 to 21.6 CAD BTDC advances the IDT from 0.91 to 7.08 CAD BTDC. However, with further advancing SOI from 21.6 to 36 CAD BTDC, the IDT starts to retard toward 4.46 CAD BTDC due to the spray over-dilution.
2. Advancing the SOI shifts the major HRR mode to the lean mixtures and the LTC conditions by increasing the LTC contribution from 33.9 % to 76.7%, while the peak HRR is reduced.
3. For the earliest SOI the formed ignition kernels are either non-existent or small in size, leading to possible premixed flame initiation challenges.
4. The ignition index analysis showed that while advanced SOI reduces the peak HRR and leads to smaller ignition kernels, it also creates mixture stratification within lean/stoichiometric conditions, which in turn creates reactivity stratification within the spray. In retrospect, such a stratified mixture could be ignited by utilizing a second pilot injection closer to the TDC (e.g., SOI-7.2 case).

CRediT authorship contribution statement

Bulut Tekgül: Conceptualization, Methodology, Software, Formal analysis, Writing - original draft, Visualization. **Heikki Kahila:** Conceptualization, Writing - review & editing. **Shervin Karimkashi:** Conceptualization, Writing - original draft. **Ossi Kaario:** Supervision, Writing - review & editing. **Éric Lendormy:** Conceptualization, Methodology. **Jari Hyvönen:** Conceptualization, Methodology. **Ville Vuorinen:** Conceptualization, Supervision, Funding acquisition, Writing - review & editing.

Declaration of Competing Interest

The authors declare that they have no known competing financial interests or personal relationships that could have appeared to influence the work reported in this paper.

Acknowledgments

The present study has been financially and academically supported by the Wärtsilä Finland Oy and the Academy of Finland (Grant Nos. 318024 and 297248). The computational resources for this study were provided by CSC – Finnish IT Center for Science. The first author has been financially supported by the Merenkulun Säätiö. We thank Dr. Minh Bau Luong for his help in compression heating model implementation.

References

[1] Reitz RD. Directions in internal combustion engine research. Combust Flame 2013; 160(1):1–8. https://doi.org/10.1016/j.combustflame.2012.11.002.
[2] Reitz RD, Duraisamy G. Review of high efficiency and clean reactivity controlled compression ignition (RCCI) combustion in internal combustion engines. Prog Energy Comb Sci 2015;46:12–71. https://doi.org/10.1016/j.pecs.2014.05.003.
[3] Paykani A, Kakaee AH, Rahnama P, Reitz RD. Progress and recent trends in reactivity-controlled compression ignition engines. Int J Engine Res 2016;17(5): 481–524. https://doi.org/10.1177/1468087415593013.
[4] Dempsey AB, Reitz RD. Computational optimization of reactivity controlled compression ignition in a heavy-duty engine with ultra low compression ratio. SAE Int J Engines 2011;4(2):2222–39. https://doi.org/10.4271/2011-24-0015.
[5] Paykani A, Garcia A, Shahbakhti M, Rahnama P, Reitz RD. Reactivity controlled compression ignition engine: pathways towards commercial viability. Appl Energy 2021;282:116174. https://doi.org/10.1016/j.apenergy.2020.116174.

[6] Kahila H, Wehrfritz A, Kaario O, Vuorinen V. Large-eddy simulation of dual-fuel ignition: diesel spray injection into a lean methane-air mixture. Combust Flame 2019;199:131–51. https://doi.org/10.1016/j.combustflame.2018.10.014.

[7] Liu X, Kokjohn S, Wang H, Yao M. A comparative numerical investigation of reactivity controlled compression ignition combustion using Large Eddy Simulation and Reynolds-Averaged Navier-Stokes approaches. Fuel 2019;257:116023. https://doi.org/10.1016/j.fuel.2019.116023.

[8] Kahila H, Kaario O, Ahmad Z, Ghaderi Masouleh M, Tekgül B, Larmi M, et al. A large-eddy simulation study on the influence of diesel pilot spray quantity on methane-air flame initiation. Combust Flame 2019;206:506–21. https://doi.org/10.1016/j.combustflame.2019.05.025.

[9] Tekgül B, Kahila H, Kaario O, Vuorinen V. Large-eddy simulation of dual-fuel spray ignition at different ambient temperatures. Combust Flame 2020;215:51–65. https://doi.org/10.1016/j.combustflame.2020.01.017.

[10] Kokjohn SL, Hanson RM, Splitter DA, Reitz RD. Fuel reactivity controlled compression ignition (RCCI): a pathway to controlled high-efficiency clean combustion. Int J Engine Res 2011;12(3):209–26. https://doi.org/10.1177/1468087411401548.

[11] Dempsey AB, Walker NR, Gingrich E, Reitz RD. Comparison of low temperature combustion strategies for advanced compression ignition engines with a focus on controllability. Combust Sci Technol 2014;186(2):210–41. https://doi.org/10.1080/00102202.2013.858137.

[12] Tong L, Wang H, Zheng Z, Reitz R, Yao M. Experimental study of RCCI combustion and load extension in a compression ignition engine fueled with gasoline and PODE. Fuel 2016;181:878–86. https://doi.org/10.1016/j.fuel.2016.05.037.

[13] Liu H, Tang Q, Ran X, Fang X, Yao M. Optical diagnostics on the reactivity controlled compression ignition (RCCI) with micro direct-injection strategy. Proc Combust Inst 2019;37(4):4767–75. https://doi.org/10.1016/j.proci.2018.06.180.

[14] Liu H, Tang Q, Yang Z, Ran X, Geng C, Chen B, Feng L, Yao M. A comparative study on partially premixed combustion (PPC) and reactivity controlled compression ignition (RCCI) in an optical engine. Proc Combust Inst 2019;37(4):4759–66. https://doi.org/10.1016/j.proci.2018.06.004.

[15] Liu X, Kokjohn S, Li Y, Wang H, Li H, Yao M. A numerical investigation of the combustion kinetics of reactivity controlled compression ignition (RCCI) combustion in an optical engine. Fuel 2019;241:753–66. https://doi.org/10.1016/j.fuel.2018.12.068.

[16] Kakaee AH, Jafari P, Paykani A. Numerical study of natural gas/diesel reactivity controlled compression ignition combustion with large eddy simulation and reynolds-averaged Navier-Stokes model. Fluids 2018;3(2):24. https://doi.org/10.3390/fluids3020024.

[17] Jin T, Wu Y, Wang X, Luo KH, Lu T, Luo K, Fan J. Ignition dynamics of DME/methane-air reactive mixing layer under reactivity controlled compression ignition conditions: effects of cool flames. Appl Energy 2019;249:343–54. https://doi.org/10.1016/j.apenergy.2019.04.161.

[18] Yu GH, Luong MB, Chung SH, Yoo CS. Ignition characteristics of a temporally evolving n-heptane jet in an iso-octane/air stream under RCCI combustion-relevant conditions. Combust Flame 2019;208:299–312. https://doi.org/10.1016/J.COMBUSTFLAME.2019.07.011.

[19] Luong MB, Yu GH, Chung SH, Yoo CS. Ignition of a lean PRF/air mixture under RCCI/SCCI conditions: a comparative DNS study. Proc Combust Inst 2017;36(3):3623–31. https://doi.org/10.1016/j.proci.2016.08.038.

[20] Luong MB, Yu GH, Chung SH, Yoo CS. Ignition of a lean PRF/air mixture under RCCI/SCCI conditions: chemical aspects. Proc Combust Inst 2017;36(3):3587–96. https://doi.org/10.1016/j.proci.2016.06.076.

[21] Luong MB, Sankaran R, Yu GH, Chung SH, Yoo CS. On the effect of injection timing on the ignition of lean PRF/air/EGR mixtures under direct dual fuel stratification conditions. Combust Flame 2017;183:309–21. https://doi.org/10.1016/j.combustflame.2017.05.023.

[22] Bhagatwala A, Sankaran R, Kokjohn S, Chen JH. Numerical investigation of spontaneous flame propagation under RCCI conditions. Combust Flame 2015;162(9):3412–26. https://doi.org/10.1016/j.combustflame.2015.06.005.

[23] Zhou D, Yang W, Zhao F, Li J. Dual-fuel RCCI engine combustion modeling with detailed chemistry considering flame propagation in partially premixed combustion. Appl Energy 2017;203:164–76. https://doi.org/10.1016/j.apenergy.2017.06.021.

[24] Karimkashi S, Kahila H, Kaario O, Larmi M, Vuorinen V. A numerical study on combustion mode characterization for locally stratified dual-fuel mixtures. Combust Flame 2020;214:121–35. https://doi.org/10.1016/j.combustflame.2019.12.030.

[25] Wang Z, Zhao Z, Wang D, Tan M, Han Y, Liu Z, Dou H. Impact of pilot diesel ignition mode on combustion and emissions characteristics of a diesel/natural gas dual fuel heavy-duty engine. Fuel 2016. https://doi.org/10.1016/j.fuel.2015.11.077.

[26] Li Y, Jia M, Liu Y, Xie M. Numerical study on the combustion and emission characteristics of a methanol/diesel reactivity controlled compression ignition (RCCI) engine. Appl Energy 2013;106:184–97. https://doi.org/10.1016/j.apenergy.2013.01.058.

[27] Weller HG, Tabor G, Jasak H, Fureby C. A tensorial approach to computational continuum mechanics using object-oriented techniques. Comput Phys 1998;12(6):620. https://doi.org/10.1063/1.168744.

[28] Jasak H, Weller HG, Gosman AD. High resolution NVD differencing scheme for arbitrarily unstructured meshes. Int J Numer Methods Fluids 1999;31(2):431–49. https://doi.org/10.1002/(SICI)1097-0363(19990930)31:2<431::AID-FLD884>3.0.CO;2-T.

[29] Wehrfritz A, Kaario O, Vuorinen V, Somers B. Large Eddy simulation of n-dodecane spray flames using flamelet generated manifolds. Combust Flame 2016;167:113–31. https://doi.org/10.1016/j.combustflame.2016.02.019.

[30] Kahila H, Wehrfritz A, Kaario O, Ghaderi Masouleh M, Maes N, Somers B, et al. Large-eddy simulation on the influence of injection pressure in reacting Spray A. Combust Flame 2018;191:142–59. https://doi.org/10.1016/j.combustflame.2018.01.004.

[31] Kaario OT, Vuorinen V, Kahila H, Im HG, Larmi M. The effect of fuel on high velocity evaporating fuel sprays: Large-Eddy simulation of Spray A with various fuels. Int J Engine Res 2019. https://doi.org/10.1177/1468087419854235.

[32] Engine Combustion Network. Combustion Research Facility, Sandia National Laboratories, Livermore, CA; 2019.https://ecn.sandia.gov.

[33] Yao T, Pei Y, Zhong BJ, Som S, Lu T, Luo KH. A compact skeletal mechanism for n-dodecane with optimized semi-global low-temperature chemistry for diesel engine simulations. Fuel 2017;191:339–49. https://doi.org/10.1016/j.fuel.2016.11.083.

[34] Niemeyer KE, Curtis NJ, Sung CJ. pyJac: analytical Jacobian generator for chemical kinetics. Comput Phys Commun 2017;215:188–203. https://doi.org/10.1016/j.cpc.2017.02.004. arXiv:1605.03262.

[35] Hairer E, Wanner G. Solving Ordinary Differential Equations II, vol. 14. Springer-Verlag; 1996. https://doi.org/10.1007/978-3-662-09947-6.

[36] Hawkes ER, Somers B. Ignition and flame structure – model results & analysis (in spray A), 5th Engine Combustion Network Workshop, Detroit, MI, USA; 2017.

[37] Varna A, Wehrfritz A, Hawkes ER, Cleary MJ, Lucchini T, D'Errico G, Kook S, Chan QN. Application of a multiple mapping conditioning mixing model to ecn spray a. Proc Combust Inst 2019;37(3):3263–70. https://doi.org/10.1016/j.proci.2018.06.007.

[38] Pei Y, Hawkes ER, Bolla M, Kook S, Goldin GM, Yang Y, Pope SB, Som S. An analysis of the structure of an n-dodecane spray flame using TPDF modelling. Combust Flame 2016;168:420–35. https://doi.org/10.1016/j.combustflame.2015.11.034.

[39] Kundu P, Ameen MM, Som S. Importance of turbulence-chemistry interactions at low temperature engine conditions. Combust Flame 2017;183:283–98. https://doi.org/10.1016/j.combustflame.2017.05.025.

[40] Bhagatwala A, Chen JH, Lu T. Direct numerical simulations of HCCI/SACI with ethanol. Combust Flame 2014;161(7):1826–41. https://doi.org/10.1016/j.combustflame.2013.12.027.

[41] Heywood JB. Internal combustion engine fundamentals. New York: McGraw-Hill; 1988.

[42] Goodwin DG, Speth RL, Moffat HK, Weber BW. Cantera: An object-oriented software toolkit for chemical kinetics, thermodynamics, and transport processes, https://www.cantera.org, version 2.4.0; 2018.https://doi.org/10.5281/zenodo.1174508.

[43] Wehrfritz A, Vuorinen V, Kaario O, Larmi M. Large eddy simulation of high-velocity fuel sprays: studying mesh resolution and breakup model effects for spray A. Atomiz Sprays 2013;23(5):419–42. https://doi.org/10.1615/AtomizSpr.2013007342.

[44] Pei Y, Som S, Pomraning E, Senecal PK, Skeen SA, Manin J, Pickett LM. Large eddy simulation of a reacting spray flame with multiple realizations under compression ignition engine conditions. Combust Flame 2015;162(12):4442–55. https://doi.org/10.1016/j.combustflame.2015.08.010.

[45] Pettinen R, Kaario O, Larmi M. Dual-fuel combustion characterization on lean conditions and high loads, SAE Technical Paper; 2017.https://doi.org/10.4271/2017-01-0759.

[46] Borghesi G, Krisman A, Lu T, Chen JH. Direct numerical simulation of a temporally evolving air/n-dodecane jet at low-temperature diesel-relevant conditions. Combust Flame 2018;195:183–202. https://doi.org/10.1016/j.combustflame.2018.02.020.

[47] Mastorakos E. Ignition of turbulent non-premixed flames. Prog Energy Combust Sci 2008;35(1):57–97. https://doi.org/10.1016/j.pecs.2008.07.002.